

Imaging of microwave permittivity, tunability, and damage recovery in (Ba,Sr)TiO₃ thin films

D. E. Steinhauer,^{a)} C. P. Vlahacos, F. C. Wellstood, and Steven M. Anlage
Center for Superconductivity Research, Department of Physics, University of Maryland, College Park, Maryland 20742-4111

C. Canedy and R. Ramesh
Department of Materials and Nuclear Engineering, University of Maryland, College Park, Maryland 20742-2115

A. Stanishevsky and J. Melngailis
Department of Electrical Engineering, University of Maryland, College Park, Maryland 20742-3285

(Received 27 July 1999; accepted for publication 15 September 1999)

We describe the use of a near-field scanning microwave microscope to quantitatively image the dielectric permittivity and tunability of thin-film dielectric samples on a length scale of 1 μm . We demonstrate this technique with permittivity images and local hysteresis loops of a 370-nm-thick Ba_{0.6}Sr_{0.4}TiO₃ thin film at 7.2 GHz. We also observe the role of annealing in the recovery of dielectric tunability in a damaged region of the thin film. We can measure changes in relative permittivity ϵ_r , as small as 2 at $\epsilon_r = 500$, and changes in dielectric tunability $d\epsilon_r/dV$ as small as 0.03 V⁻¹. © 1999 American Institute of Physics. [S0003-6951(99)00446-5]

Many techniques exist for quantitatively measuring the dielectric permittivity of thin-film samples. For example, thin-film capacitors allow measurement of the in-plane^{1,2} and normal^{3,4} components of the permittivity tensor. Dielectric resonators⁵ and Corbino measurements⁶ have also been used. However, thin-film capacitors require the sample to be altered, possibly affecting the dielectric permittivity; most other methods either require bulk samples or have poor spatial resolution. Recently, near-field techniques, based on coaxial cavity⁷⁻⁹ microwave probes which use the reflected microwave signal from a sample, have been used to determine the dielectric constant ϵ_r and tunability (i.e., how ϵ_r depends on voltage) of thin films. However, no quantitative tunability measurements at high spatial resolution have been demonstrated. In this letter, we present a nondestructive, noninvasive near-field scanning microwave microscope¹⁰⁻¹³ which can quantitatively image the local permittivity and tunability of dielectric thin films with a spatial resolution of 1 μm .

Our near-field scanning microwave microscopes consist of an open-ended coaxial probe with a sharp, protruding center conductor (Fig. 1). The probe is connected to a coaxial transmission line resonator, which is coupled to a microwave source through a capacitive coupler. The probe tip, which has a radius $\sim 1 \mu\text{m}$ (see the inset to Fig. 1), is held fixed, while the sample is supported by a spring-loaded cantilever applying a controlled normal force of about 50 μN between the probe tip and the sample. Due to the concentration of the microwave fields at the tip, the boundary condition of the resonator, and hence, the resonant frequency f_0 and quality factor Q , are perturbed depending on the dielectric properties of the region of the sample immediately beneath the probe tip. We monitor this perturbation with a feedback circuit^{10,11}

which receives the reflected microwave signal from the resonator, keeps the microwave source locked onto the chosen resonance, and outputs the frequency shift (Δf) and Q of the resonator. We have shown that the spatial resolution of the microscope in this mode of operation is about 1 μm .¹² In addition, a local dc electric field can be applied to the sample by means of a bias tee in the resonator.

To observe the microscope's response to sample dielectric permittivity ϵ_r , we monitored the frequency shift signal while scanning samples with known ϵ_r . With well-characterized 500- μm -thick bulk dielectrics, we observed

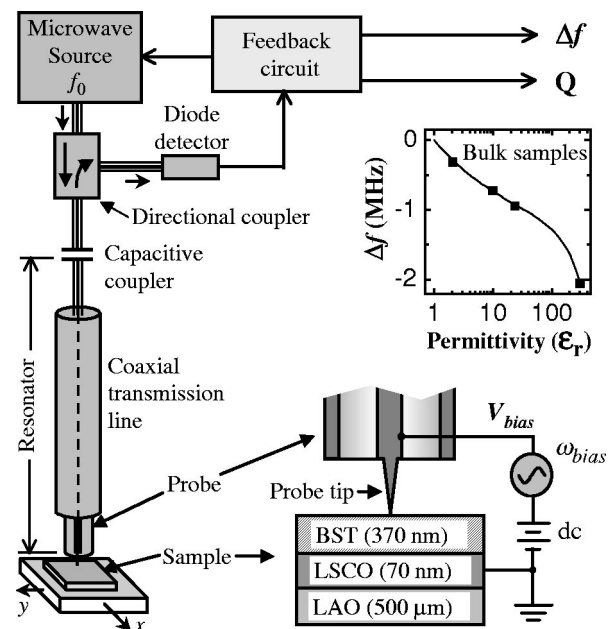


FIG. 1. Schematic of the near-field microwave microscope, with a sharp-tipped, open-ended coaxial probe (see inset). The graph shows the data (rectangles) and model results (line) of frequency shift (Δf) vs permittivity for 500- μm -thick bulk samples at 7.2 GHz.

^{a)}Electronic mail: steinhau@squid.umd.edu. Color versions of the figures in this paper can be found at http://www.csr.umd.edu/research/hifreq/micr_microscopy.html.

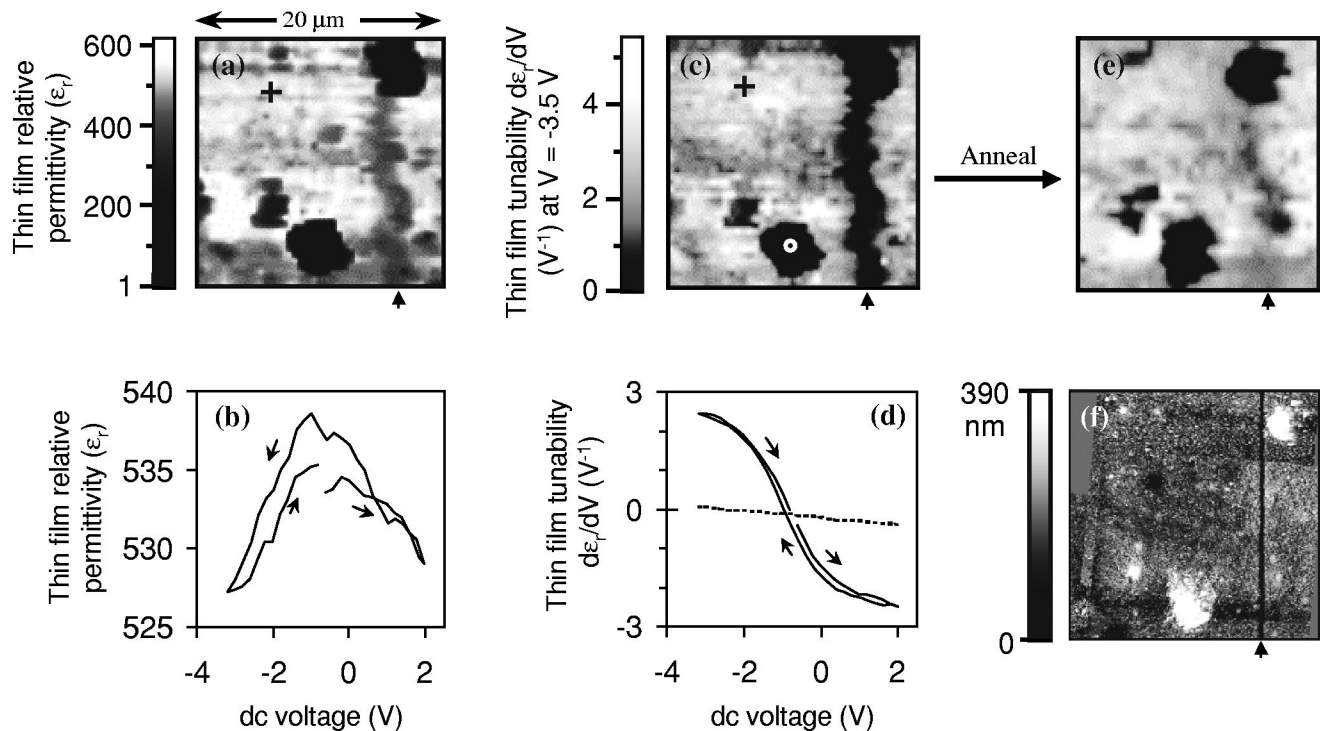


FIG. 2. Images and hysteresis loops at 7.2 GHz of the BST/LSCO/LAO thin-film sample (see the inset to Fig. 1). All images show the same $20 \times 20 \mu\text{m}^2$ area of the sample. (a) Permittivity image. (b) Hysteresis loop taken at the location marked “+” in (a). (c) Dielectric tunability image. (d) Dielectric tunability hysteresis loops. The solid line corresponds to the “+” in (c), while the dashed line corresponds to the “O” in (c). (e) Dielectric tunability image taken after the sample was annealed at 650°C in air for 20 min; note the change from (c). (f) Atomic force microscope topographic image. The milled vertical line marked by the arrow in (f) appears rough in (a) and (c) because of drift in the microscope during scanning.

that the microscope frequency shift monotonically increases in the negative direction with increasing sample permittivity (see the graph inset, Fig. 1).¹³ We observed similar behavior with thin-film samples.

For comparison, we did a finite-element calculation of the rf electric field near the probe tip. Because the probe tip radius is much less than the wavelength ($\lambda \sim 4$ cm at 7 GHz), a static calculation of the electric field is sufficient. Cylindrical symmetry further simplifies the problem to two dimensions. We represent the probe tip as a cone with a blunt end, held at a potential of $\phi = 1$ V. Using relaxation methods we solved Poisson’s equation for the potential, $\nabla^2 \phi = 0$, on a rectangular grid representing the region around the probe tip. The two variables we used to represent the properties of the probe were the aspect ratio of the probe tip ($\alpha \equiv dz/dr$) and the radius r_0 of the blunt end.

Since the sample represents a small perturbation to the resonator, we can use perturbation theory¹⁴ to find the change in the resonant frequency:

$$\frac{\Delta f}{f} \approx \frac{\epsilon_0(\epsilon_{r2} - \epsilon_{r1})}{4W} \int_{V_s} \mathbf{E}_1 \cdot \mathbf{E}_2 dV, \quad (1)$$

where \mathbf{E}_1 and \mathbf{E}_2 , and ϵ_{r1} and ϵ_{r2} are the unperturbed and perturbed electric fields, and relative permittivities of two samples, respectively; W is the energy stored in the resonator; and V_s is the volume of the sample. Using four bulk samples with known relative permittivities between 2.1 and 305, and fixing $r_0 = (0.6 \mu\text{m})/\alpha$, we used α as a fitting parameter to obtain agreement between the model results from

Eq. (1) and our data at 7.2 GHz (see the graph in Fig. 1); we found agreement to within 10% for several different probe tips, with $1.0 < \alpha < 1.7$.

To extend this model to thin films, we extend the finite-element calculation to include a thin film on top of the dielectric substrate. Once the α parameter of a probe is determined using the bulk calibration described above, we use the thin-film model combined with Eq. (1), integrating over the volume of the thin film, to obtain a functional relationship between Δf and the permittivity of the thin film. Using this model, we found that for high-permittivity ($\epsilon_r \geq 50$) thin films, the microwave microscope is primarily sensitive to the in-plane component of the permittivity tensor.

Figure 2(a) shows a quantitative permittivity ϵ_r image of a sample (see the inset to Fig. 1) consisting of a 370 nm $\text{Ba}_{0.6}\text{Sr}_{0.4}\text{TiO}_3$ (BST) thin film on a 70 nm $\text{La}_{0.95}\text{Sr}_{0.05}\text{CoO}_3$ (LSCO) counterelectrode. The substrate is LaAlO_3 (LAO). The films were made by pulsed-laser deposition at 700°C , in 200 mTorr of O_2 . The film is paraelectric at room temperature ($T_c \sim 250$ K). We measured the film thickness using scanning ion microscope images of cross sections milled by focused ion beam (FIB). To identify the scanned area on the sample, a $0.1\text{-}\mu\text{m}$ -wide line was FIB milled through the BST layer. This fiducial mark allowed further analysis of the area of interest with an atomic force microscope (AFM) [Fig. 2(f)]. In the microwave permittivity image [Fig. 2(a)], the milled line (marked by an arrow) is visible as a low-permittivity vertical band. Two low-permittivity defects are also visible. The average value of the permittivity of the film far from any defects is $\epsilon_r = 510$, in reasonable agreement with typical measurements of ϵ_r in similar films.^{2,3}

To measure the local dielectric tunability of thin films, we apply a dc electric field to the sample by voltage biasing (V_{bias}) the probe tip (see Fig. 1). A grounded metallic counterelectrode layer immediately beneath the dielectric thin film acts as a ground plane. To prevent the counterelectrode from dominating the microwave measurement, thus minimizing its effect on the microwave fields (we ignored the counterelectrode in our static field model), the sheet resistance of the counterelectrode should be as high as possible. In our case, we use LSCO with a thickness of 70 nm, giving a sheet resistance $\sim 400 \Omega/\square$. We have confirmed by experiment and model calculation¹⁰ that the contribution of the counterelectrode to the frequency shift is small ($\Delta f < 30$ kHz) relative to the contribution from a dielectric thin film with thickness > 100 nm ($\Delta f > 200$ kHz).

We first examined the tunability of the dielectric properties at a fixed point on the sample [marked by a “+” in Fig. 2(a); the resulting hysteresis loop is shown in Fig. 2(b)]. As expected, the permittivity goes down when a voltage is applied. The inverted “V” curve is centered at a bias of -0.6 V rather than 0 V probably because the asymmetric electrodes (a thin film on the bottom, and a sharp tip on top) induce unequal charges on the two surfaces.⁴ The tunability of $\sim 2\%$ is small compared to measurements on similar films (20%–30%) using standard techniques.^{1,4} The cause of this low tunability is unclear, but may be due to the microscope measuring an off-diagonal component of the nonlinear permittivity (ϵ_r , measured in the horizontal direction, while the applied field is in the vertical direction).

To image the tunability of the sample, we modulate the bias voltage applied to the probe tip at a frequency $\omega_{\text{bias}} = 1$ kHz and amplitude ± 1 V (see the inset to Fig. 1), and monitor the component of the microscope frequency shift signal at ω_{bias} with a lock-in amplifier. This ω_{bias} component is proportional to $d\epsilon_r/dV$, where V is the applied voltage. An image of $d\epsilon_r/dV$ at $V = -3.5$ V is shown in Fig. 2(c). We note that the tunability diminishes near the FIB milled line and two large defects. Figure 2(d) shows hysteresis loops at a high-permittivity location and at a low-permittivity defect, marked by the “+” and “O” symbols in (c), corresponding to the solid and dashed lines in (d), respectively. As shown in (c) and (d), the tunability at the defect is small relative to the rest of the film. The small amount of hysteresis observed is probably due to the broadened ferroelectric transition in thin films, which may be due to variations in stoichiometry and the transition temperature.

After annealing the sample at 650°C in air for 20 min, we scanned the sample again, as shown in the $d\epsilon_r/dV$ image in Fig. 2(e). The milled line, which is prominent in Fig. 2(c), is nearly invisible in (e), indicating that the dielectric tunability near the milled line has been almost completely restored.

The AFM image in Fig. 2(f) shows many of the features seen in the microwave microscope images (a) and (c). The gallium FIB milled vertical line is visible, as well as the two large low-permittivity defects, which are shown to be particles on the surface in (f). These defects are probably non-vapor-phase particles which accrued during pulsed-laser deposition. They appear slightly larger in the microwave mi-

croscope images, indicating that the spatial resolution of the microscope in this case is about $1 \mu\text{m}$. The dark horizontal bands next to the large defects are artifacts of the AFM imaging technique. We also note that the AFM image, which was acquired after the microwave images, does not show any evidence of scratching by the microscope probe tip.

The microwave technique we use is sensitive to both film thickness and permittivity. As a result, the permittivity of the large defects in Fig. 2(a) is underestimated due to the change in film thickness at these locations. However, by examining the AFM image [Fig. 2(f)], topographic features can be readily distinguished from permittivity features. Far from large topographic features in Fig. 2(f), the AFM data indicate a rms surface roughness of about 2 nm (when the data are averaged over the microwave microscope spatial resolution of $1 \mu\text{m}$), which would result in an error of $\Delta\epsilon_r \sim 1.5$ in ϵ_r data. This is much less than the observed variation $\Delta\epsilon_r \sim 30$ indicating that this observed variation in ϵ_r is real.

We can calculate the sensitivity of the microwave microscope by observing the noise in the dielectric permittivity and tunability data. For a 370-nm-thick film on a 500- μm -thick LAO substrate, with an averaging time of 40 ms, we find that the relative dielectric permittivity sensitivity is $\Delta\epsilon_r = 2$ at $\epsilon_r = 500$, and the tunability sensitivity is $\Delta(d\epsilon_r/dV) = 0.03 \text{ V}^{-1}$.

In conclusion, we have demonstrated the use of a near-field scanning microwave microscope to quantitatively image the local permittivity and tunability of dielectric thin films with a spatial resolution of $1 \mu\text{m}$.

This work has been supported by NSF-MRSEC Grant No. DMR-9632521, NSF Grant Nos. ECS-9632811 and DMR-9624021, and by the Maryland Center for Superconductivity Research.

¹B. H. Hoerman, G. M. Ford, L. D. Kaufmann, and B. W. Wessels, *Appl. Phys. Lett.* **75**, 2248 (1998).

²W. Chang, J. S. Horwitz, A. C. Carter, J. M. Pond, S. W. Kirchoefer, C. M. Gilmore, and D. B. Chrisey, *Appl. Phys. Lett.* **74**, 1033 (1999).

³Q. X. Jia, X. D. Wu, S. R. Foltyn, and P. Tiwari, *Appl. Phys. Lett.* **66**, 2197 (1995).

⁴F. A. Miranda, C. H. Mueller, C. D. Cabbage, and K. B. Bhasin, *IEEE Trans. Appl. Supercond.* **5**, 3191 (1995).

⁵A. T. Findikoglu, C. Doughty, S. M. Anlage, Qi Li, X. X. Xi, and T. Venkatesan, *J. Appl. Phys.* **76**, 2937 (1994).

⁶J. C. Booth, D. H. Wu, and S. M. Anlage, *Rev. Sci. Instrum.* **65**, 2082 (1994).

⁷Y. Cho, A. Kirihara, and T. Saeki, *Rev. Sci. Instrum.* **67**, 2297 (1996).

⁸C. Gao and X.-D. Xiang, *Rev. Sci. Instrum.* **69**, 3846 (1998).

⁹H. Chang, I. Takeuchi, and X.-D. Xiang, *Appl. Phys. Lett.* **74**, 1165 (1999).

¹⁰D. E. Steinhauer, C. P. Vlahacos, S. K. Dutta, F. C. Wellstood, and S. M. Anlage, *Appl. Phys. Lett.* **71**, 1736 (1997).

¹¹D. E. Steinhauer, C. P. Vlahacos, S. K. Dutta, F. C. Wellstood, and S. M. Anlage, *Appl. Phys. Lett.* **72**, 861 (1998).

¹²S. M. Anlage, D. E. Steinhauer, C. P. Vlahacos, B. J. Feenstra, A. S. Thanawalla, W. Hu, S. K. Dutta, and F. C. Wellstood, *IEEE Trans. Appl. Supercond.* **9**, 4127 (1999).

¹³C. P. Vlahacos, D. E. Steinhauer, S. K. Dutta, B. J. Feenstra, S. M. Anlage, and F. C. Wellstood, *Microsc. and Anal.* (in press).

¹⁴H. M. Altschuler, in *Handbook of Microwave Measurements II*, edited by M. Sucher and J. Fox (Polytechnic Institute of Brooklyn, Brooklyn, New York, 1963), pp. 530–533.